

An efficient algorithm for shadowing effect simulation under hexagonal lattice-based model

Xiaolong Jiang(蒋晓龙), Xin Xiang(向欣), Xiaoyu Luan(栾晓雨), Haijun Wang(王海军), Baoshen Jia(贾宝申), Qinghua Deng(邓青华), Chuanchao Zhang(张传超), Wei Liao(廖威), Wei Ni(倪卫), and Qihua Zhu(朱启华)
Citation: Chin. Phys. B, 2026, 35 (**8**): 086801. DOI: 10.1088/1674-1056/ae82e5
http://cpb.iphy.ac.cn; http://iopscience.iop.org/cpb

What follows is a list of articles you may be interested in

Sandwich-structured long-wave infrared transparent electromagnetic shielding film using transmittance-enhanced wetting layer/Ag stacked conductive layers

Zhirui Zhang(张智睿), Yuyang Zhang(张雨阳), Le Zhao(赵乐), Zhi Wang(王植), Chi Zhang(张弛), Yao Wu(吴尧), Ruifan Li(李瑞凡), Yonghao Han(韩永昊), and Chaoquan Hu(胡超权)
Chin. Phys. B, 2026, 35 (**4**): 046803. DOI: 10.1088/1674-1056/ae44f5

Combining machine learning algorithms with traditional methods for resolving the atomic-scale dynamic structure of monolayer MoS_2 in high-resolution transmission electron microscopy

Yu Meng(蒙宇), Shuya Wang(王淑雅), Xibiao Ren(任锡标), Han Xue(薛涵), Xuejun Yue(岳学军), Chuanhong Jin(金传洪), Shanggang Lin(林上港), and Fang Lin(林芳)
Chin. Phys. B, 2025, 34 (**1**): 016802. DOI: 10.1088/1674-1056/ad9ba3

Atomic-level quantitative analysis of electronic functional materials by aberration-corrected STEM

Wanbo Qu(曲万博), Zhihao Zhao(赵志昊), Yuxuan Yang(杨宇轩), Yang Zhang(张杨), Shengwu Guo(郭生武), Fei Li(李飞), Xiangdong Ding(丁向东), Jun Sun(孙军), and Haijun Wu(武海军)
Chin. Phys. B, 2024, 33 (**11**): 116802. DOI: 10.1088/1674-1056/ad7afc

Evolutionary algorithm for optimization of multilayer coatings

Mahdi Ebrahimi, Mohsen Ghasemi, Zeinab Sajjadi
Chin. Phys. B, 2018, 27 (**10**): 106802. DOI: 10.1088/1674-1056/27/10/106802

Cryo-ET bridges the gap between cell biology and structural biophysics

Xiao-Fang Cheng(程小芳), Rui Wang(王睿), Qing-Tao Shen(沈庆涛)
Chin. Phys. B, 2018, 27 (**6**): 066803. DOI: 10.1088/1674-1056/27/6/066803

An efficient algorithm for shadowing effect simulation under hexagonal lattice-based model

Xiaolong Jiang(蒋晓龙)†, Xin Xiang(向欣), Xiaoyu Luan(栾晓雨), Haijun Wang(王海军), Baoshen Jia(贾宝申), Qinghua Deng(邓青华), Chuanchao Zhang(张传超), Wei Liao(廖威), Wei Ni(倪卫), and Qihua Zhu(朱启华)

Laser Fusion Research Center, China Academy of Engineering Physics, Mianyang 621900, *China*

(Received 8 May 2026; revised manuscript received 8 June 2026; accepted manuscript online 26 June 2026)

This paper introduces an efficient algorithm for simulating the shadowing effect in hexagonal-lattice networks, addressing a critical gap in existing methods that are limited to cubic-lattice models. The shadowing effect significantly influences roughness development in processes such as film growth and plasma etching but has previously been impractical for hexagonal lattices due to its computational complexity. The proposed algorithm dramatically reduces computational load by strategically reducing the calculation dimensionality from three-dimensional (3D) to two-dimensional (2D) and handling the misaligned odd and even layers separately. This enables simulations on personal computers, with the typical simulation time decreasing from several days to less than one hour (achieving $> 100\times$ acceleration). Validated simulations show consistent results with cubic-lattice models in both growth (roughening) and etching (smoothing) scenarios, while demonstrating superior symmetry in roughness formation. The work facilitates broader applications of shadowing simulations and integration with other hexagonal-lattice-based mechanisms.

Keywords: thin film structure and morphology, Monte Carlo method, lattice theory and statistics, algorithm

PACS: 68.55.−a, 02.50.Ng, 05.50.+q, 02.60.Gf

DOI: 10.1088/1674-1056/ae82e5 **CSTR:** 32038.14.CPB.ae82e5

1. Introduction

Shadowing effect is a very important mechanism that greatly shapes the growth/etching front in processes such as film growth and plasma etching.[1–4] It describes the phenomenon in which taller features of a fluctuating surface tend to block incoming flux from reaching lower-lying areas. For deposition processes, shadowing gives rise to roughness growth in the sense that once surface fluctuations are initialized by noise, local peaks consistently grow faster than valleys because they receive more incident particles than the valleys.[1,3,4] For etching processes, however, more etchant arriving at local peaks leads to a higher etching rate than at valleys, and therefore tends to smooth any existing roughness.[2] Shadowing-induced roughness generally manifests as random surface structures at micro/nano-scale dimensions. Traditionally, this roughening effect degrades component performance, making it a long-standing challenge in plasma etching technologies for decades.[5–12] In recent years, however, this effect has been actively leveraged in surface micro/nano-texturing, gradually demonstrating broad prospects in optics, environmental science, and biotechnology.[13–18]

To achieve an understanding and tailored control of surface roughness for varying application scenarios, it is essential to establish theoretical simulation models for surface morphology evolution. Current simulations predominantly employ the Monte Carlo method.[1–4,19,20] This approach represents the etching/deposition substrate as a hexagonal- or cubic-lattice network, using Monte Carlo techniques to generate stochastic etching or deposition particles. Specifically, the initial position and movement direction of an incident particle are randomly selected, followed by trajectory calculations to determine the collision lattice on the etching/deposition surface. Material is then removed (etching) or added (deposition) at the collision lattice, ultimately evolving the etching profile. Among these steps, the calculation of the collision lattice is the core component of the entire simulation. The efficiency of this algorithm directly determines the computational performance of the simulation process.

Notably, the calculation method of the collision lattice is intrinsically linked to the adopted lattice network model. The most popular lattice models include cubic and hexagonal lattices. The cubic-lattice model features a simpler algorithm but is only applicable to crystalline substrates with well-defined cubic-lattice orientations.[19,20] It fails to provide adequate symmetry or isotropy for non-cubic-lattice or amorphous materials without straightforward lattice representations. This limitation exists in many practically interesting etching/deposition processes, for example, glass (fused silica, K9 glass, etc.), metal masks (Al, Cr, etc.), organic coatings (photoresist, polydimethylacrylamide (PDMA), poly(methyl methacrylate) (PMMA), etc.) in etching processes, and most common dielectric films (SiO_2, HfO_2, MgF_2, etc.) in deposition processes. The hexagonal-lattice model overcomes these limitations with broader applicability.[21,22] However, due to

†Corresponding author. E-mail: xljiang@caep.cn

© 2026 Chinese Physical Society and IOP Publishing Ltd. All rights, including for text and data mining, AI training, and similar technologies, are reserved.

inherent offsets between rows and layers in hexagonal lattices, numerical processing of lattice coordinates and trajectory calculations becomes significantly more complex and computationally costly. Consequently, to the author's knowledge, no reported models currently exist for shadowing effect simulation in plasma etching or film growth processes based on a hexagonal-lattice network. This gap has hindered the advancement of shadowing effect simulations, as well as their integration with other hexagonal-lattice-based models, such as kinetic mechanisms.[23]

To address these challenges, we propose an efficient algorithm for hexagonal-lattice-based shadowing effect simulation. It can dramatically reduce computational load and enable simulations on personal computers. Using this algorithm, the authors have successfully completed hexagonal-lattice-based shadowing growth and etching simulations with a typical simulation time of one hour or less for one standard time unit (achieving $> 100\times$ acceleration over brute-force methods). The simulation results are consistent with those obtained using the cubic-lattice model, while demonstrating superior symmetry in mound formation. This breakthrough opens avenues for complex substrate modeling in plasma etching and nanotexturing, with future extensions toward multi-mechanism integration.

2. Modelling framework

2.1. Difficulty of hexagonal-lattice-based shadowing effect simulation

Figure 1 illustrates the schematic of the shadowing effect under cubic-lattice and hexagonal-lattice models. The key part of the simulation is determining which lattice of the undulating surface is collided with by the incident particle. The most straightforward method to do so is to calculate the perpendicular distance between the particle trajectory and the center of each lattice. If the distance is less than one lattice unit size, a collision will occur; otherwise, no collision happens. Since all lattice units above the "ground" could potentially be collided with, for a $(2+1)$-dimensional model, each incident particle requires $N \times N \times (\mathrm{PV}+1)$ rounds of distance calculations, where N is the simulation resolution and PV is the peak–valley value of surface topography. Considering the duty cycle of surface structures, a reasonable estimation is $0.5 \times N^2 \times (\mathrm{PV}+1)$ counts. According to literature reports and the authors' preliminary research, PV of the shadowed growth surface increases linearly with deposition layers in the form of $k*$time/layer, where $k = 1$ for cosine distribution and $k = 2$–3 for isotropic distribution. To ensure sufficient roughness growth, the number of simulation time/layers is generally at least on the order of the simulation resolution N. Consequently, the required number of distance calculations for one incident particle scales as $\sim N^3$, with one complete simulation involving $\sim N^6$ calculation counts ($N \times N$ deposited particles per layer and $\sim N$ layers for one complete simulation).

For the cubic-lattice-based model, reducing the calculation count for determining the collision lattice is straightforward because there are no offsets between adjacent rows and layers. Since all morphology layers share the same X and Y coordinates, one can easily eliminate the Z-dimension calculation by representing each lattice column with the local morphology height and comparing it with the local flight altitude of the incident particle. Further reduction in computational complexity is also feasible, thanks to the concise representation of lattice coordinates. For the hexagonal-lattice-based model, however, none of the aforementioned simplified methods are applicable.

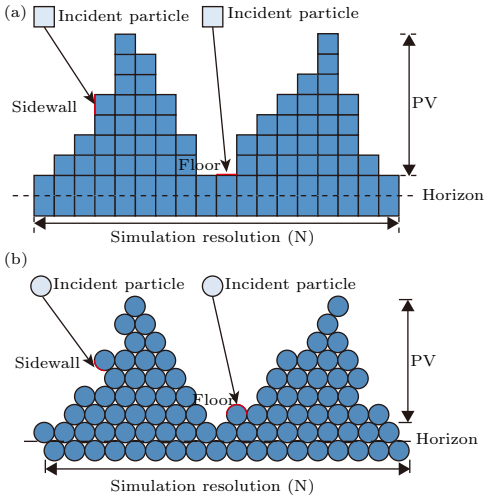


Fig. 1. Schematic of the shadowing effect calculation (side view). (a) Cubic-lattice-based model; (b) hexagonal-lattice-based model.

2.2. Modelling algorithm

The algorithm proposed in this paper is illustrated in Fig. 2. The core methodology involves the following steps: First, it resolves the interlayer offset issues by splitting the hexagonal lattice into odd and even layers for independent collision calculations. The final collision lattice is selected from the obtained odd and even collision lattices based on the "shortest flight distance" principle. This separated calculation approach dramatically reduces the difficulty of numerical processing. Second, the proposed method pre-filters a large number of lattice columns that cannot possibly be collided with by calculating the distances between the particle trajectory and the even/odd lattice columns and excluding the columns with trajectory-column distances greater than one lattice size. Thus, the possible collision area is quickly located with minimal computational effort.

The specific simulation process is as follows:

Step 1: Initialize or import an existing hexagonal-lattice-based three-dimensional surface morphology, which is described by a two-dimensional matrix $H(x,y)$ representing the local height of each pixel in lattice space.

Coordinating surface morphology in lattice space makes numerical processing of surface morphology much easier and more straightforward. When lattice coordinates in physical space are needed, they can be easily calculated as follows:

$$x' = x \times \text{size_lattice_}x + \text{mod}\,(x+1,2) \times \text{offset_}x,$$
$$y' = y \times \text{size_lattice_}y - \text{mod}\,(x+z,1) \times \text{offset_}y,$$
$$z' = z \times \text{size_lattice_}z,$$

where x', y', and z' represent physical space coordinates, and x, y, and z represent lattice space coordinates. $\text{Size_lattice_}x = \sqrt{3}/2$, $\text{size_lattice_}y = 1$, and $\text{size_lattice_}z = \sqrt{6}/3$ represent the lattice sizes in the x, y, and z dimensions, respectively. The parameters $\text{offset_}x = \sqrt{3}/3$ and $\text{offset_}y = 0.5$ denote the offsets in the x and y directions caused by the parity of the z and x/y coordinates, respectively.

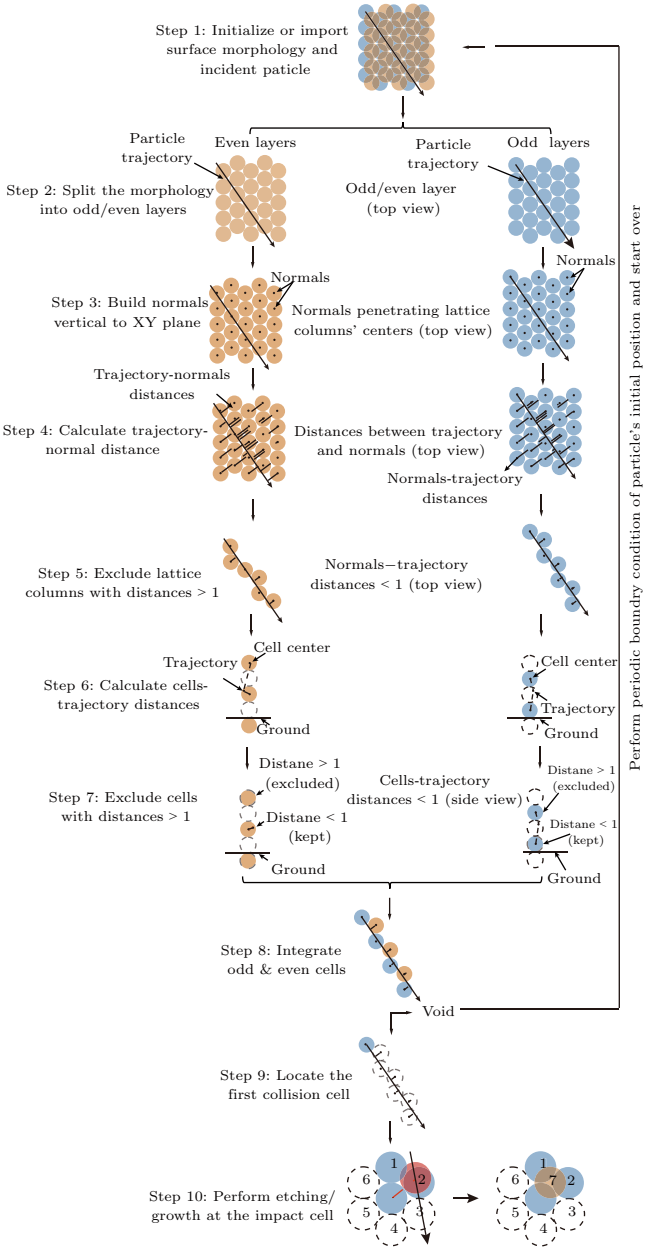


Fig. 2. Schematic diagram of the hexagonal-lattice-based shadowing effect simulation algorithm.

The $\text{mod}\,(x,b)$ function returns the remainder of x divided by b, which is used here to determine parity. The transition relationship is illustrated in Fig. 3.

Step 2: Split the lattice network of surface morphology into odd-layer and even-layer subsets according to the heights of stacked layers. The heights of the odd-layer ($H(x,y)_{\text{odd}}$) and even-layer ($H(x,y)_{\text{even}}$) subsets are calculated as follows:

$$H(x,y)_{\text{odd}} = H(x,y) - \text{mod}\,(H(x,y),2),$$
$$H(x,y)_{\text{even}} = H(x,y) - \text{mod}\,(H(x,y)+1,2),$$

where $H(x,y)_{\text{odd}}$ and $H(x,y)_{\text{even}}$ represent the local heights of (x,y) in the odd-layer and even-layer sets, respectively. Splitting the misaligned odd and even layers decouples the subsequent calculations, thus making the numerical processing much more straightforward.

Step 3: Establish normals to the XY plane passing through the lattice centers, as shown in Fig. 4(a). Note that the normal establishment, as well as the following calculations, is performed in physical space. Therefore, it is necessary to calculate the (x,y) coordinates of the central points of odd/even-layer lattice cells in physical space beforehand. The calculation method is described in Step 1.

Step 4: Calculate the perpendicular distance between the normals and the particle trajectory. The calculation method is illustrated in Fig. 4(b). First, locate the projection line of the particle trajectory on the XY plane, and then calculate the distance from the lattice center to the projection line.

Step 5: Exclude lattices with normal–trajectory distances greater than one lattice size. These cells are too far away from the trajectory line and would not be collided with. Thus, only a ribbon of lattice columns is retained. Consequently, the trajectory collision calculation problem is reduced from three dimensions to two dimensions.

Step 6: In the following steps, we further locate the collided lattice cell on each lattice column. Similarly, the criterion is whether the cell–trajectory distance exceeds one lattice unit size. In this step, the perpendicular distance from the lattice cells to the trajectory line (marked as d_1) is calculated. Since lattice cells underneath the surface would never be collided with because they are blocked by superficial cells, this portion of cells is omitted in the cell–trajectory distance calculations.

Step 7: Exclude the cells with cell–trajectory distances greater than one lattice unit size. Note that, since lattice cells are discretely distributed along the Z-axis only in odd/even-layer subsets, a scenario may occur in which, although the normal–trajectory distance is less than 1, no collided cell exists in some columns. On the other hand, it is also possible that more than one collided cell exists in a single lattice column. In this case, the cell with the larger Z-coordinate value is selected, because incident particles always enter from top to bottom and the higher lattice is collided with first.

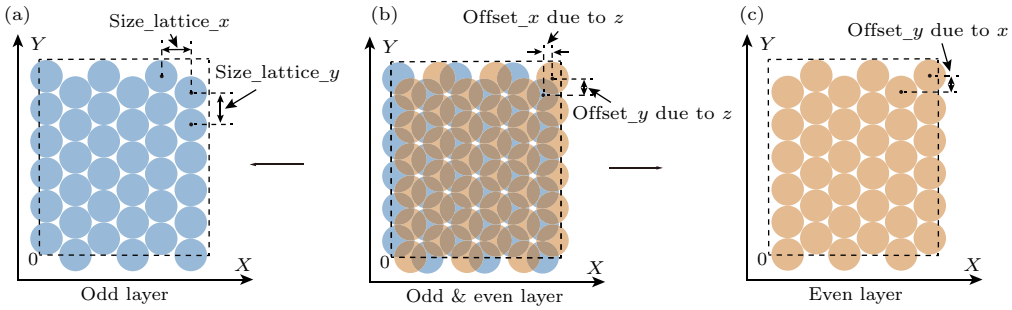


Fig. 3. Schematic diagram of the conversion relationship between lattice-space coordinates and physical-space coordinates for odd and even layers.

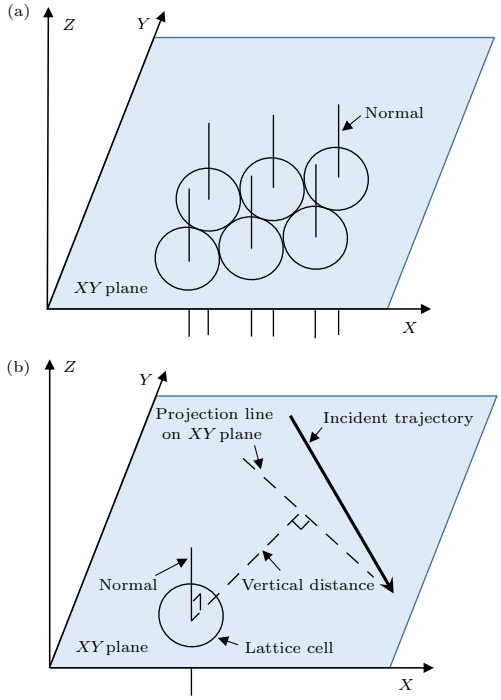


Fig. 4. Schematic diagram of (a) normal establishment and (b) calculation of the normal–trajectory distance.

Step 8: After the collided lattice in each lattice column is separately located, we integrate these two subsets of collided cells for the following calculations. There may be situations where both subsets are empty because incident particles do not descend to sufficient depth. In this case, the initial position of the incident particle is updated through periodic boundary conditions, and the simulation returns to Step 1 to restart the iteration.

Step 9: The task of this step is to determine the first collided cell, i.e., the cell closest to the initial position of the incident particle. The key part of this determination, as shown in Fig. 5(a), is to calculate the distance traveled by the incident particle from its initial position until collision occurs [Collision occurs when the distance from the particle center to the cell center equals one lattice unit size]. The specific calculation algorithm is illustrated in Fig. 5(b). The traveled distance d is computed as follows:

$$d_3 = \boldsymbol{V}\cdot\boldsymbol{V}_1/|\boldsymbol{V}_1|,\ \ d_2 = \sqrt{1-{d_1}^2},\ \ d = d_3 - d_2,$$

where $\boldsymbol{V}$ represents the vector from the initial position of the particle center to the lattice center, $\boldsymbol{V}_1$ represents the trajectory vector of the incident particle, and d_3 represents the projected component of the particle–lattice distance on the trajectory vector. The lattice unit size is defined as 1 standard size in the simulation. The value of d_1 is obtained in Step 6.

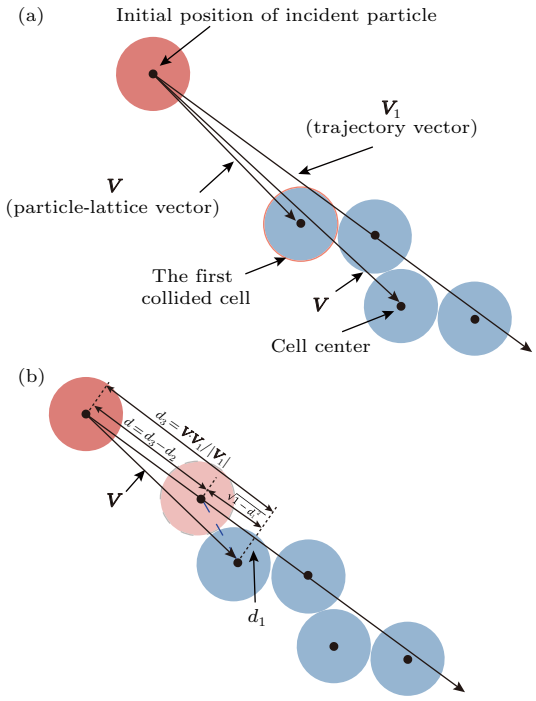


Fig. 5. Schematic diagram of (a) the identification of the first collided lattice and (b) the calculation method of the distance traveled by the incident particle from its initial position until collision occurs.

Step 10: In this step, etching or growth is performed at the impact cell. For the etching process, material removal is executed at the collided cell. For the growth process, the incident particle descends until landing on one of the adjacent cells of the collided cell. In the hexagonal-lattice-based model, each lattice cell has twelve adjacent cells: six at the same layer and three at both the upper and lower layers. In Fig. 6(a), cells 1–6 are in the same layer (i.e., the middle layer), and cells 7–9 are in the upper layer. The lower-layer cells are not visible in the diagram due to spatial overlap with the upper-layer cells. Each middle-layer cell covers a 60° range, while each upper/lower-layer cell covers a 120° range. When a collision occurs, the incident particle occupies an adjacent vacancy according to the

relative angle of the contact point. Figures 6(b)–6(g) show the determination process of the impact cell under different scenarios.

Case 1: If the target cell is vacant, the incident particle directly occupies the target cell.

Case 2: If the target cell is already occupied, the incident particle takes the corresponding vacancy in the upper layer.

Case 3: If the target cell is already occupied and the secondly targeted upper-layer cell is not adequately supported — that is, its three underlying cells are not fully occupied — the incident particle slides into this middle-layer vacancy.

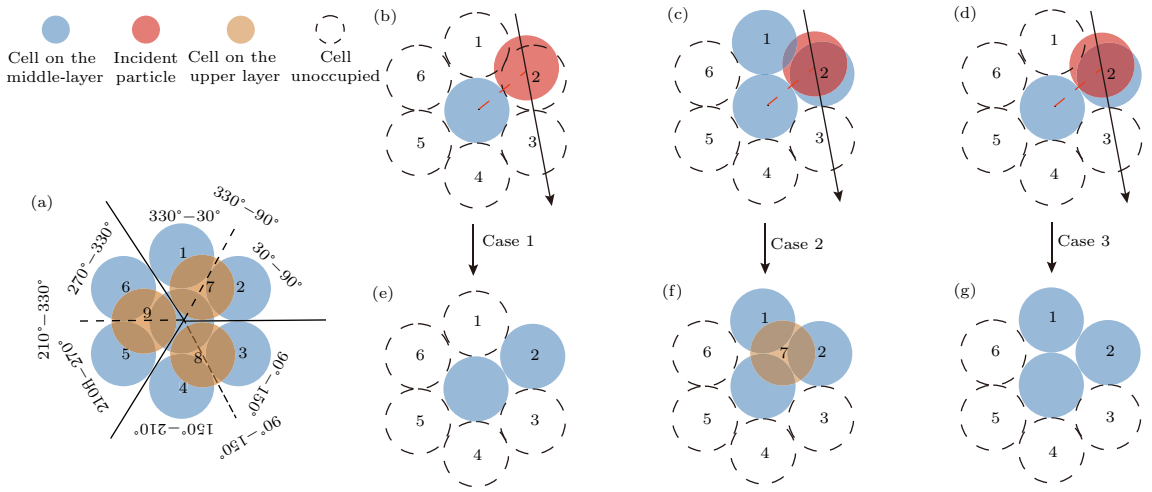


Fig. 6. The determination process of the impact cell in the growth process under different scenarios. (a) Schematic diagram of the adjacent cells. Lattice morphology (b)–(d) before landing and (e)–(g) after landing.

3. Simulation results and discussion

Using the proposed approach, shadowing effects during growth and etching processes are successfully simulated on a personal computer. It is found that a simulation with a resolution of 256×256 takes about one hour for a single standard time unit (an average of one deposited particle per lattice cell), while simulations with resolutions of 128×128 and 64×64 take 5–10 min and less than one minute, respectively. Therefore, one round of 256×256 resolution simulation takes several days, whereas simulations at 128×128 and 64×64 resolutions take several hours and less than one hour, respectively. In comparison, using the traditional distance calculation method, a simulation with a resolution of 256×256 for one standard time unit takes several days, and one complete simulation would theoretically take about years.

Note that the real resolution of the hexagonal-lattice model is larger than the nominal resolution. For the hexagonal-lattice model, samples with a cell resolution of $N \times N$ and lattice constant d correspond to rectangles with dimensions $(N \times \sqrt{3}/2 \times d) \times (N \times d)$ in reality. Therefore, we choose a lattice resolution of $(N/\sqrt{3}/2) \times N$, and after simulation, convert it into a cubic $N \times N$ height matrix through interpolation.

3.1. Shadowing growth

Shadowing growth is an important micro-process in film deposition and plasma etching. It generally gives rise to surface roughening in the form of mound growth. After a certain point, only one mound stands out and becomes remarkably larger than the others. The reason for this phenomenon is that shadowing is an inherently nonlocal process. The shadowing of a surface feature depends on the heights of all other surface features, not only on nearby or local ones. The taller the surface feature, the more incident particles it receives. The impact of the shadowing effect on surface roughness has been intensively studied through both experimental measurements [3,4,7] and theoretical modeling.[1–4,19,20] Generally, it gives rise to surface roughness featuring periodic mounds with well-defined separation. The number of mounds decreases, while both their height and width increase over time. This ultimately leads to a mounded surface dominated by one distinctly large mound.

Using the proposed algorithm, morphology evolution under shadowing growth is simulated and compared with simulation results obtained based on the cubic-lattice-based simulation in our previous work,[19] which represent the aforementioned findings reported in the literature. The proposed hexagonal-lattice model generates consistent simulation results with the cubic-lattice model. As shown in Fig. 7, the proposed algorithm effectively captures the mound evolution process, characterized by the emergence, growth, and coalescence of random mounds. Furthermore, compared with the cubic-lattice model, the mounds generated by the hexagonal-lattice model are closer to being circular, exhibiting higher symmetry.

Figure 8 presents the surface roughness analysis results of Fig. 7, focusing on how the PV value, rms roughness, and surface autocorrelation length evolve with time. According to

findings in the literature, the PV value, rms roughness, and autocorrelation length increase linearly with time. The PV and rms values of a surface quantify the vertical fluctuations of roughness, but they do not provide information on the lateral dimension. The autocorrelation length is the lateral length beyond which surface heights are not significantly correlated. For a mounded surface, the correlation length is a measure of the mean width of the mounds. As shown in Figs. 8(a)–8(c), the PV value, rms roughness, and autocorrelation length obtained by this method increase linearly with time, similar to the cubic-lattice-based model. Specifically, as shown in Fig. 8(c), the hexagonal-lattice model achieves greater overlap of the autocorrelation length curves along the X, Y, and radial directions, indicating that the mound widths in the X, Y, and radial directions are more consistent. This agrees with the morphological results in Fig. 7, showing that mounds are more circular in the hexagonal model.

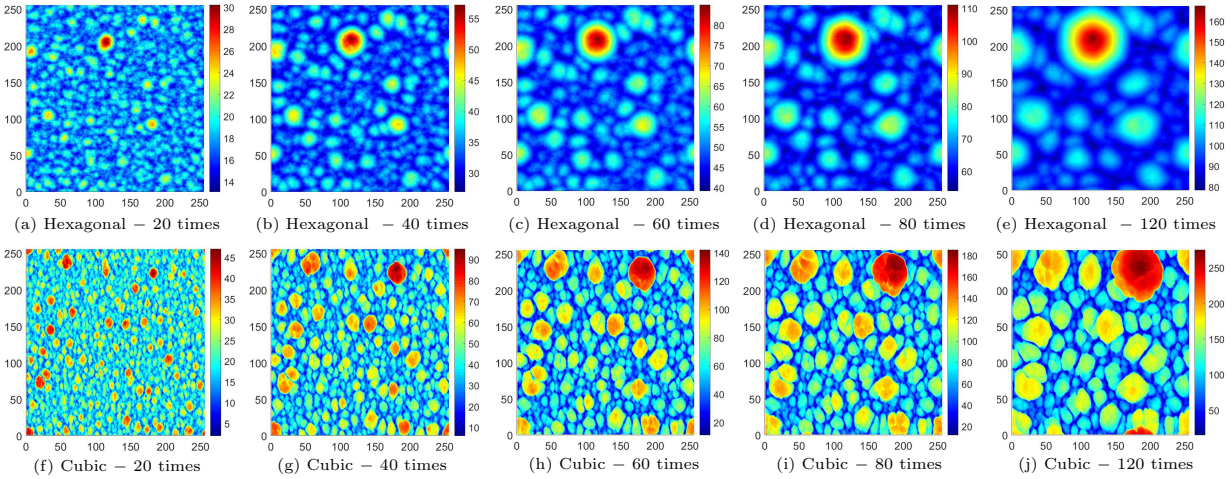


Fig. 7. Morphology evolution under isotropic shadowing growth for (a)–(e) hexagonal-lattice-based simulation in this work; (f)–(j) cubic-lattice-based simulation in our previous work.[19] Note that "times" is short for "standard time units". One standard time unit corresponds to an average of one deposited particle per lattice cell.

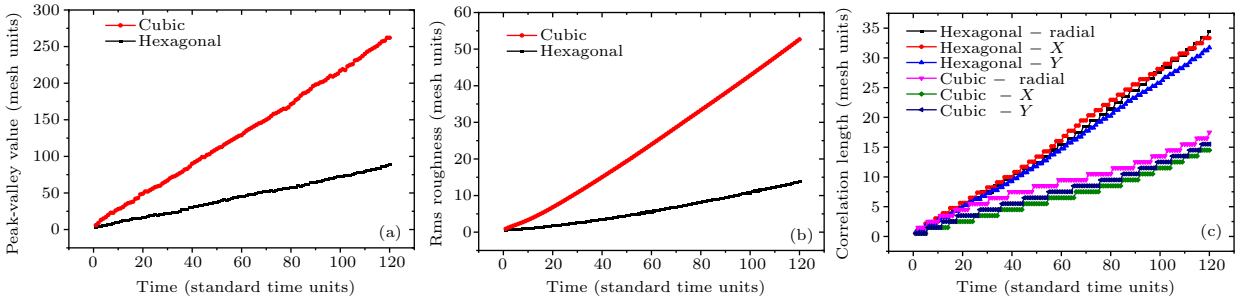


Fig. 8. Roughness analysis as a function of time for shadowing growth: (a) PV; (b) rms roughness; (c) correlation length.

It is noteworthy that in the hexagonal-lattice model, the PV value and rms roughness grow more slowly, whereas the autocorrelation length increases faster. This is primarily attributed to two factors. First, due to misalignment within the hexagonal lattice network, the equivalent lattice height in the hexagonal-lattice model is less than one lattice dimension, as in the cubic-lattice model. Second, in the hexagonal lattice model, each node is supported by three underlying lattices, whereas the cubic lattice model has only one. This allows deposited particles in the hexagonal model to relax downward until they find sufficient support when underlying support is lacking; conversely, in the cubic model — where each particle relies on a single support — this relaxation effect is much weaker.

Consequently, the hexagonal lattice promotes lateral expansion of surface mounds rather than vertical growth. This manifests as slower increases in PV and rms values but a faster increase in the autocorrelation length. It should be noted that this relaxation effect in the hexagonal lattice model can be disabled; however, it is enabled by default in this work because it aligns more closely with experimental observations in most scenarios.

3.2. Shadowing etching

In plasma etching, etching by neutral radicals is a shadowing etching process. According to the literature, shadow etching does not generate roughness; on the contrary, it tends to smooth pre-existing roughness. This is because local peaks receive more etchant particles and are thus etched faster. Figure 9 shows the morphology evolution under isotropic shad-

owing etching obtained using the proposed approach and compared with the cubic-lattice-based simulation obtained in our previous work,[19] which represents the aforementioned findings reported in the literature. Figure 10 shows the corresponding roughness analysis. As one can see, both surface morphology and roughness parameters exhibit similar evolution patterns. Specifically, the PV value and rms roughness barely increase except for the early stage, and the correlation length remains half of a lattice. Since the heights of all lattices are set to be the same (zero) at the beginning of the simulation, the initial rms roughness and PV value are zero. After etching, the PV value as well as rms roughness rapidly increases to a stable value. As for the autocorrelation length, it remains constant (half of a lattice) during the whole etching process. Since half of a lattice is the lowest value allowed for autocorrelation length in the discrete model, this means that surface morphology is totally uncorrelated, i.e., neighboring areas (neighboring columns in the simulation model) evolve independently.

Similar to shadow growth, the hexagonal lattice model yields lower PV and rms roughness values in shadowing etching; however, the underlying mechanism differs from that of shadow growth. In shadow etching, the discrepancy in roughness evolution between the hexagonal and cubic lattice models can be solely attributed to differences in their equivalent lattice heights. This is because the relaxation effect present in the hexagonal lattice applies only to depositing particles, not to etchant particles: etchant particles react upon collision rather than settling into stable sites.

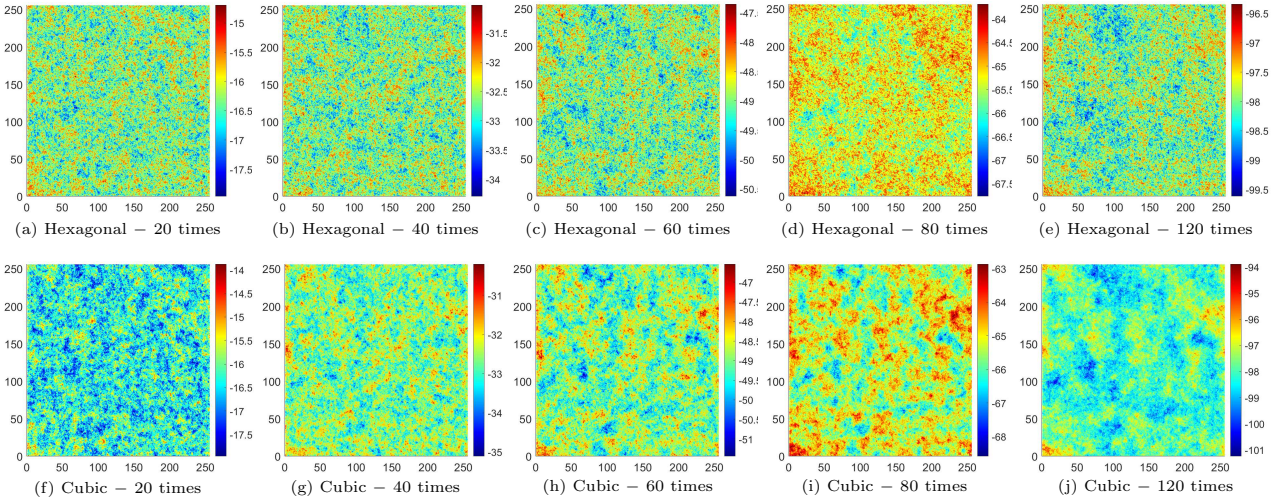


Fig. 9. Morphology evolution under isotropic shadowing etching for (a)–(e) hexagonal-lattice-based simulation in this work; (f)–(j) cubic-lattice-based simulation in our previous work.[19] Note that "times" is short for "standard time units". One standard time unit corresponds to an average of one deposited particle per lattice cell.

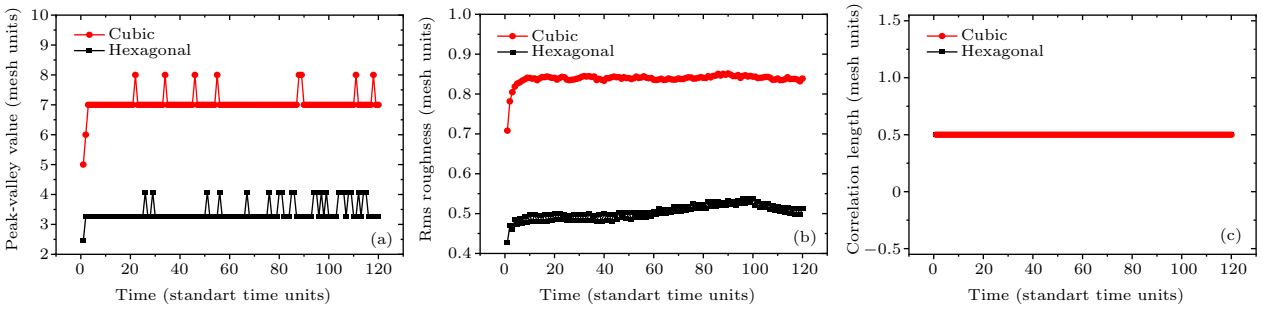


Fig. 10. Roughness analysis as a function of time for shadowing etching: (a) PV; (b) rms roughness; (c) correlation length.

4. Summary

This work resolves the long-standing challenge of simulating shadowing effects in hexagonal-lattice networks by developing an algorithm that reduces the computational load by reducing the simulation dimension from three-dimensional to two-dimensional and decoupling the calculations for misaligned odd and even layers. Key innovations include: (1) layer-parity splitting to eliminate interlayer offset constraints; (2) collision-region pre-screening via trajectory-lattice distance filtering; (3) optimized collision detection using shortest-flight-distance principles. Validated through growth and etching simulations at resolutions up to 256×256, the algorithm achieves practical runtime ($\sim$ 1 hour/standard time unit) on personal computers. Growth/etching simulations match cubic-lattice results while exhibiting superior symmetry. The framework enables unprecedented integration with other hexagonal-lattice-based mechanisms and opens avenues for modeling complex substrates in thin-film growth, plasma

etching, and surface nano-texturing. Future work will extend to multi-mechanism simulations.

Acknowledgments

Project supported by the National Natural Science Foundation of China (Grant No. 12275254) and the Laser Fusion Research Center Funds for Young Talents (Grant No. RCFPD7-2024-7).

References

[1] Karunasiri R P U, Bruinsma R and Rudnick J 1989 *Phys. Rev. Lett.* **62** 788
[2] Drotar J T, Zhao Y P, Lu T M and Wang G C 2000 *Phys. Rev. B* **62** 2118
[3] Pelliccione M, Karabacak T and Lu T M 2006 *Phys. Rev. Lett.* **96** 146105
[4] Pelliccione M, Karabacak T, Gaire C, Wang G C and Lu T M 2006 *Phys. Rev. B* **74** 125420
[5] Wang S Q, Zhou C H, Ru H Y and Zhang Y Y 2005 *Appl. Opt.* **44** 4429
[6] Zhou J, Chen Y, Zhou W L, Miao X S, Yang Z, Yu N, Liu H, Lan T and Yan J 2013 *Appl. Surf. Sci.* **280** 862
[7] Qiu R F, Lu H, Chen D J, Zhang R, Zhe Y, Yu N N, Liu H, Lan T and Yan J B 2011 *Appl. Surf. Sci.* **257** 2700
[8] Kokkoris G, Constantoudis V, Angelikopoulos P, Boulousis G and Gogolides E 2007 *Phys. Rev. E* **76** 193405
[9] Jiang X L, Liu Y, Liu Z K, Qiu K Q, Xu X D, Hong Y L and Fu S J 2015 *Appl. Surf. Sci.* **355** 1180
[10] Li L, Abe T and Esashi M 2003 *J. Vac. Sci. Technol. B* **21** 2545
[11] Choi D Y, Lee J H, Kim D S and Jung S T 2004 *J. Appl. Phys.* **95** 8400
[12] Goyal A, Hood V and Tadigadapa S 2006 *J. Non Cryst. Solids* **352** 657
[13] Hsu C H, Lo H C, Chen C F, Wu C T, Hwang J S, Das D, Tsai J, Chen L C and Chen K H 2004 *Nano Lett.* **4** 471
[14] Zheng J, Yang R, Xie L, Qu J L, Liu Y and Li X G 2010 *Adv. Mater.* **22** 1451
[15] Guo Y R, Wang T, Chen J, Zheng J, Li X G and Ostrikov K 2018 *Adv. Energy Mater.* **8** 1800085
[16] Lee S H and Lu J Q 2010 *Nanotechnology* **21** 155303
[17] Hein E, Fox D and Fouckhardt H 2011 *J. Nanophotonics* **5** 051703
[18] Mundo R D, Benedictis V D, Palumbo F and Agostino R 2009 *Appl. Surf. Sci.* **255** 5461
[19] Jiang X L, Zhang C C, Luan X Y, Tang H P, Deng Q H, Jia B S, Wang H J, Liao W, Ni W and Zhu Q H 2026 *Appl. Surf. Sci.* **715** 164617
[20] Kokkoris G and Gogolides E 2012 *J. Phys. D: Appl. Phys.* **45** 165204
[21] Bruschi P, Cagnoni P and Nannini A 1997 *Phys. Rev. B* **55** 7955
[22] Angqvist M, Magnus Rahm J, Gharaee L and Erhart P 2019 *Phys. Rev. B* **83** 073605
[23] Jiang X L, Wu L X, Yang K, Liu T X, Liao W, Zhang C C, Zhang L J, Liu Y and Jiang X D 2021 *Appl. Surf. Sci.* **543** 148862